Available online at www.sciencedirect.com
SCIENCE DIRECT
Polymer 46 (2005) 5125–5132
polymer
www.elsevier.com/locate/polymer

Synthesis and characterization of multi-walled carbon nanotubes reinforced polyamide 6 via in situ polymerization

Chungui Zhao[a], Guanjun Hu[a], Ryan Justice[b], Dale W. Schaefer[b], Shimin Zhang[a], Mingshu Yang[a,*], Charles C. Han[a]

[a]*Key Laboratory of Engineering Plastics, Joint Laboratory of Polymer Science and Materials, Institute of Chemistry, Chinese Academy of Sciences, Beijing 100080, China*
[b]*Department of Chemical and Materials Engineering, University of Cincinnati, Cincinnati, OH 45221-0012, USA*

Received 29 December 2004; accepted 20 April 2005

Abstract

Polyamide 6 (PA6)/carbon nanotubes (PA6/CNTs) composites have been prepared by in situ polymerization of ε-caprolactam in the presence of pristine and carboxylated multi-walled carbon nanotubes (MWNT and MWNTCOOH). Viscosity measurements show that adding 0.5 wt% of carbon nanotubes (CNTs) does not affect the molecular weight of PA6. Compared with pure PA6, the yield strength of PA6/CNTs composites loaded with 0.5 wt% CNTs is almost unchanged, and the tensile strength is increased slightly. Dynamic mechanical analysis (DMA) demonstrates that both the storage modulus (E') and glass transition temperature (T_g) of the PA6/CNTs composites increase, particularly for PA6/MWNTCOOH, indicating there is some chemical bonding between PA6 and MWNTCOOH. Scanning electron microscopy (SEM), transmission electron microscopy (TEM) and ultra small-angle X-ray scattering (USAXS) show that MWNT and MWNTCOOH are well dispersed in PA6 matrix. Comparison of the USAXS data with a stiff-rod model and wormlike rod model reveals that the CNTs are quite flexible, regardless the degree of chemical modification. Due to the flexibility of CNTs, mechanical properties of the PA6/CNTs composites are marginally enhanced.

Keywords: Carbon nanotubes; PA6; Dispersion

1. Introduction

Since Iijima [1] reported their discovery in 1991, carbon nanotubes (CNTs) have been recognized as ideal reinforcing fillers for polymers due to their unique mechanical properties and high aspect ratio [2]. Multi-walled carbon nanotubes (MWNT) show a tensile strength as high as 200 GPa, and a Young's modulus as high as 1 TPa [3] with an aspect ratio of about 1000. Many researchers have concentrated on the fabrication of CNTs reinforced polymer composites [4,5]. Several methods have been developed to fabricate polymer/CNTs composites, including solution compounding [6–9], melt compounding [10–16] and in situ polymerization [17–22].

Numerous studies stress the role of dispersion and interfacial interactions in the properties of polymer/CNTs composites. Matsuo et al. [7] reported the preparation of ultrahigh molecular weight polyethylene (UHMWPE)/MWNT composites by solution compounding. These composites exhibited high electric conductivity, high Young's modulus and 100-fold elongation. Sun and coworkers [9] prepared poly(vinyl alcohol) (PVA)-functionalized CNTs through esterification, and followed by solution compounding to fabricate PVA/CNTs composites. The CNTs were homogeneously dispersed and the mechanical properties of composites were significantly improved. Kuma et al. [17] added single-walled carbon nanotubes (SWNT) in poly(phosphoric acid) (PPA) to synthesize poly(*p*-phenylene benzobisoxazole) (PBO)/SWNT composite fibers using typical PBO polymerization conditions. The tensile strength of PBO fiber was increased by 50% by addition of 10 wt% SWNT. Castaño et al. [18] used oxidized MWNT to fabricate PMMA/MWNT composites by bulk polymerization. Raman and infrared

* Corresponding author. Tel.: +86 10 82615665; fax: +86 10 62559373.
E-mail address: yms@iccas.ac.cn (M.S. Yang).

0032-3861/$ - see front matter © 2005 Elsevier Ltd. All rights reserved.
doi:10.1016/j.polymer.2005.04.065

spectroscopy confirmed chemical bonding between PMMA and MWNT. The composites showed significant reinforcement effect: by adding only 1 wt% of oxidized MWNT, storage modulus (E') at 90 °C increased by 1135% and the glass transition temperature (T_g) increased about 40 °C.

Notwithstanding the properties improvements cited above, other studies show marginal mechanical improvement in polymer/CNTs composites [5]. That is to say, the potential of CNTs as reinforcement for polymers has not been fully realized [4]. Polyamide 6 (PA6) is an important engineering plastic that falls in this category. Wang et al [23] modified MWNT using an ultrasonically initiated in situ emulsion polymerization to obtain polymer-encapsulated CNTs, which were then, melt compounded with PA6. They found that polymer-encapsulated MWNT could be successfully dispersed in PA6. By adding 1 wt% polymer-encapsulated MWNT, the tensile strength and Young's modulus of composites improved by 30 and 35% respectively. Liu et al. [16] prepared PA6/MWNT nanocomposites by a simple melt compounding; they found a homogenous dispersion of MWNT and strong interfacial adhesion between MWNT and PA6. The yield strength and Young's modulus was increased by about 214 and 162%, respectively at 2 wt% loading. Due to the unusual method of sample preparation, however, the absolute values, (47.2 and 1240 MPa, respectively) were much lower than the common PA6 resins (ca. 80 and 2500 MPa respectively) [24]. Friedrich and coworkers [14] fabricated PA6/MWNT/ABS three-element blends by melt compounding. The tensile strength increased by 27% but elongation at break decreased significantly at a high MWNT loading of 8 wt%.

In this paper, we report an in situ polymerization method to produce PA6/CNTs composites using pristine and carboxylated MWNT. CNTs are ultrasonically dispersed in a mixture of ε-caprolactam and H_2O to form a homogeneous polymerizable master solution. Then additional ε-caprolactam is added to obtain PA6/CNTs composites using typical PA6 hydrolytic polymerization conditions. The effect of CNTs on the tensile, dynamic mechanical and crystallization properties is investigated. Dispersion state of CNTs in PA6 is characterized by scanning electron microscopy (SEM), transmission electron microscopy (TEM) and ultra small-angle X-ray scattering (USAXS). The morphology of CNTs in PA6 matrix is analyzed using USAXS data. The origin of the observed marginal reinforcement effect in PA6/CNTs composites is then discussed.

2. Experimental

2.1. Materials

Multi-walled carbon nanotubes (MWNT), with diameter of 20–40 nm and length of ca. 10 μm, were purchased from Shenzhen Nanotech Port Co., Ltd (Shenzhen, China). The carboxylated MWNT (MWNTCOOH) were obtained by treating MWNT with concentrated nitric acid [25]. The –COOH content in MWNTCOOH was about 1 carboxyl group per 50 carbon atoms as determined by chemical titration [26]. Polymerization grade ε-caprolactam (chemical formula: $C_6H_{11}NO$) was purchased from Ube Industries, Ltd and used as received.

2.2. In situ polymerization

3.0 g CNTs (MWNT or MWNTCOOH), 60 g ε-caprolactam and 60 g H_2O were mixed and ultrasonicated for 0.5 h to form a polymerizable master solution. Then the master solution (123 g) and additional ε-caprolactam (540 g) were mixed in a 2 l closed autoclave for the hydrolytic polymerization. The polymerization temperature was maintained at 230 °C for 2 h, 245 °C for 2 h, and then increased to 265 °C for 2.5 h. Flowing nitrogen atmosphere was maintained to exhaust water during the last 1.5 h. The products were removed from the autoclave, palletized, extracted five times with boiling water (2 h per each extraction), and dried in vacuum at 110 °C for at least 8 h. The resulting PA6/CNTs composites contain ca. 0.5 wt% CNTs (MWNT or MWNTCOOH) and are denoted as PA6/MWNT and PA6/MWNTCOOH, respectively. Those formulations were chosen because no significant improvements were obtained at higher CNTs loading by simple melt compounding. For the sake of comparison, pure PA6 was synthesized under the same conditions.

2.3. Characterization

2.3.1. Molecular weight

Molecular weight of the pure PA6 and the PA6/CNTs composites was determined by measuring the viscosity of corresponding solution (0.5 g/100 ml) in concentrated sulfuric acid according to the method described by Flory [27].

2.3.2. Tensile properties

The tensile properties were measured using an Instron 3365 universal tensile tester. The tests were carried out at a crosshead speed of 10 mm/min. The cylindrical dumbbell samples were injection-molded on a CS-183 Mini-Max Molder (CSI Co. USA). The overall length was 22 mm and narrow section diameter was 1.6 mm. The data reported here represent the average of five successful tests.

2.3.3. Dynamic mechanical properties

Dynamic mechanical analysis (DMA) was performed under nitrogen atmosphere using a Perkin–Elmer DMA 7 at a heating rate of 5.0 °C/min; the dynamic temperature spectra were obtained in three-point bending mode at a vibration frequency of 1 Hz with temperature from −50 to 150 °C. The specimens ($3.0\times1.6\times15$ mm^3) were injection-molded on the CS-183 Mini-Max Molder.

2.3.4. Crystallization properties

Differential scanning calorimetry (DSC) measurements were conducted on a Perkin–Elmer DSC 7. The samples (ca. 5 mg) were heated to 250 °C, and maintained for 5 min to eliminate the thermal history. After conditioning the samples were cooled to 70 °C and reheated to 250 °C. Both the heating and cooling rates were 10 °C/min, and all tests were conducted in nitrogen atmosphere. The DSC data were taken during the cooling and the second heating.

2.3.5. Scanning electron microscopy

A JEOL S-4300F field emission scanning electron microscope was used for SEM observation. DMA samples of PA6/CNTs composites were quenched and fractured in liquid nitrogen; the fracture surface was sputter-coated with platinum prior to their observation. The operation voltage was 15 kV.

2.3.6. Transmission electron microscopy

TEM was carried on a Hitachi (Japan) H-800 with an acceleration voltage of 200 kV. The ultrathin slices were prepared by sectioning the DMA samples along the direction parallel to the injection under cryogenic condition.

2.3.7. Ultra small-angle X-ray scattering

Ultra small-angle X-ray scattering (USAXS) was performed using the Bonse-Hart camera at the UNICAT beam line at Argonne National Laboratory (Argonne, IL, USA). The data were desmeared using routines provided by UNICAT and reported as the absolute scattering cross section per unit sample volume per steradian. The air blank background was subtracted.

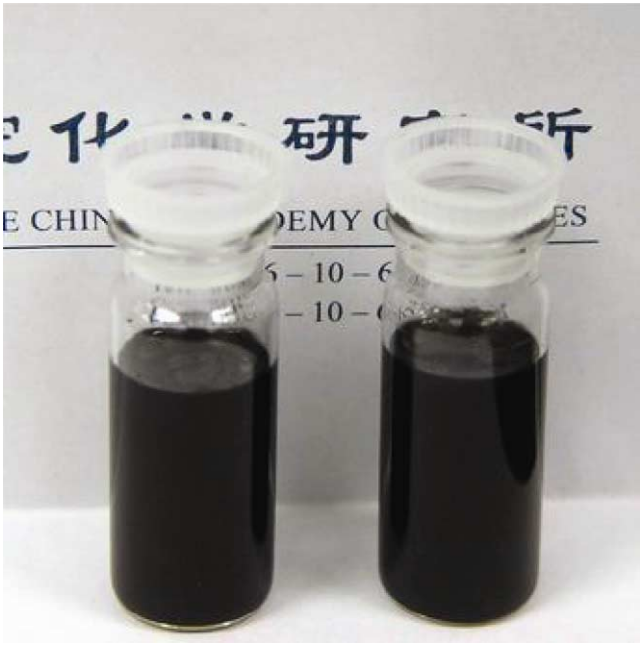

Fig. 1. MWNT (left) and MWNTCOOH (right) in the master solution after stored for 24 h. There is no evidence of phase separation or precipitation.

3. Results and discussion

3.1. Polymerizable master solution

Fig. 1 illustrates the state of CNTs in the polymerizable master solution after storage for 24 h. Both MWNT (left) and MWNTCOOH (right) are well dispersed. By contrast, only the MWNTCOOH will disperse and pristine MWNT will agglomerate and settle at the bottom in pure water.

CNTs are good electron acceptors, and can be dispersed in aromatic amines [28] and *N*-methyl-pyrrolidone [29], which act as electron donors. The PA6 monomer, ε-caprolactam, is a comparatively good electron donor, so MWNT can form an electron-transfer complex with ε-caprolactam in the master solution. These well-dispersed master solutions facilitate the formation of composites in which CNTs are homogenously dispersed.

3.2. Molecular weight

Viscosity-average molecular weight (M_η) of PA6, PA6/MWNT and PA6/MWNTCOOH are listed in Table 1. The introduction of CNTs has minimal effect on the molecular weight of PA6. It should be pointed out that CNTs cannot be separated from the solution for the viscosity measurements, so the measured values would be somewhat on the high side. This influence of CNTs on the composite solutions, however, should be insignificant due to the low loading (0.5 wt%). In fact, we did measure the viscosity of the solution of the pure PA6 sample in presence of MWNT with equal content in PA6/MWNT and found that the values did not show any significant difference (PA6 + MWNT in Table 1). Jia et al [30] reported that CNTs could block the polymerization of PA6 and reduce the molecular weight, which seems to be in contradiction with our results. The discrepancy is probably because the CNTs content in our experiments is fairly low compared to the Jia et al work (18 wt%).

3.3. Tensile properties

The tensile properties of PA6 and PA6/CNTs composites are given in Table 2. CNTs improve the tensile strength marginally, decrease the elongation at break, but have little effect on the yield strength. From the stress–strain curves (Fig. 2), one can see that the CNTs reinforced PA6 composites exhibit more obvious strain post-yield hardening than neat PA6. In addition, the carboxylation

Table 1
Viscosity average molecular weight of PA6 and PA6/CNTs composites

Samples	PA6	PA6/MWNT	PA6/MWNTCOOH	PA6 + MWNT
M_η (g/mol)	30,100	30,500	30,700	30,300

Table 2
Tensile properties of PA6 and PA6/CNTs composites.

Sample	Tensile strength (MPa)	Yield strength (MPa)	Elongation at break (%)
PA6	60.9±0.8	51.6±1.1	154±19
PA6/MWNT	65.5±1.3	52.1±1.3	131±12
PA6/MWNTCOOH	65.9±1.0	52.4±1.4	123±19

treatment has little effect on the tensile behavior of the composites.

3.4. Dynamic mechanical properties

Fig. 3 shows the storage modulus (E') and loss tangent (tan δ) for PA6 and PA6/CNTs composites as determined by dynamic mechanical analysis (DMA). CNTs increase E' of composites slightly. From loss tangent curves, glass transition temperature (T_g) increases from 45.3 °C for the neat PA6 to 57.5 and 58.5 °C for PA6/MWNT and PA6/MWNTCOOH respectively. The enhanced T_g of composites is due to confinement of the PA6 molecular segments in the proximity of CNTs. Since MWNTCOOH can bond with PA6 molecular chains during in situ polymerization, E' and T_g of PA6/MWNTCOOH are somewhat higher than PA6/MWNT.

3.5. Crystallization properties

Crystallization behavior of PA6 and PA6/CNTs composites is shown in Table 3. CNTs have no effect on the melting point (T_m) of PA6, but they do increase the crystallinity (%C). The crystallization temperature (T_c) is increased from 186.0 to 193.0 and 193.4 °C respectively for PA6/MWNT and PA6/MWNTCOOH, demonstrating that CNTs act as heterogeneous crystallization nucleator of the matrix.

The above results show that CNTs slightly affect the room-temperature mechanical properties of the composites,

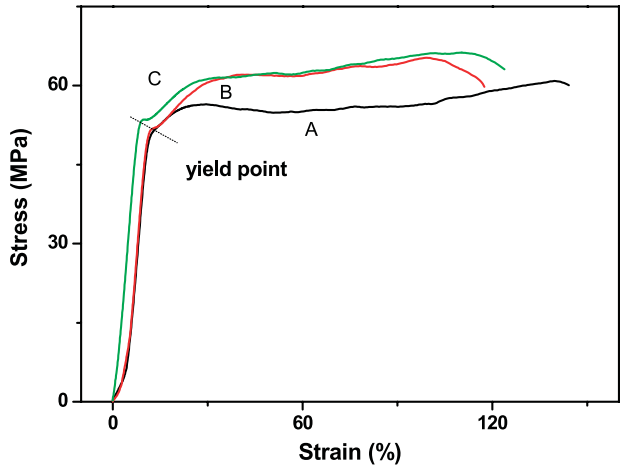

Fig. 2. Typical stress–strain curves of PA6 and PA6/CNTs composites.

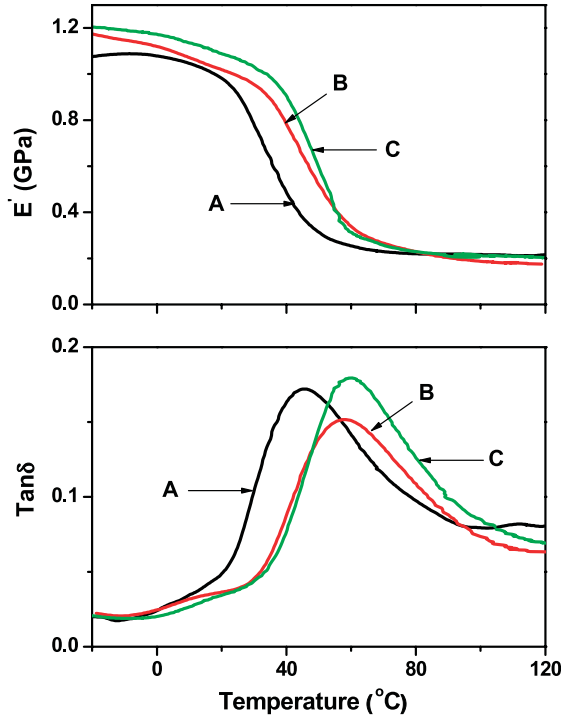

Fig. 3. Storage modulus (E') and loss tangent (tan δ) curves for PA6 and PA6/CNTs composites.

although they influence the glass transition and crystallization behavior of the matrix. This lackluster mechanical enhancement could be due to a number of factors including poor dispersion of CNTs in the matrix, alteration of the properties of the matrix by the filler, poor adhesion between the filler and the matrix and flexibility of CNTs themselves. To elucidate these issues, the dispersion state of CNTs was investigated by scanning electron microscopy (SEM), transmission electron microscopy (TEM) and ultra small-angle X-ray scattering (USAXS).

3.6. SEM and TEM

Figs. 4 and 5 present the SEM and TEM images for PA6/MWNT and PA6/MWNTCOOH respectively. Both MWNT and MWNTCOOH are well dispersed in PA6 matrix.

3.7. USAXS

The USAXS data confirm the good dispersion. Fig. 6

Table 3
Crystallization parameters of PA6 and PA6/CNTS composites measured by DSC

Sample	T_m (°C)	T_c (°C)	%C[a] (%)
PA6	219.4	186.0	27.1
PA6/MWNT	219.2	193.0	31.6
PA6/MWNTCOOH	219.9	193.4	30.7

[a] Assessed by integrating the normalized area of the melting endothermic peak and rationing the heat involved to the reference value of a 100% crystalline PA6 (240 J/g).

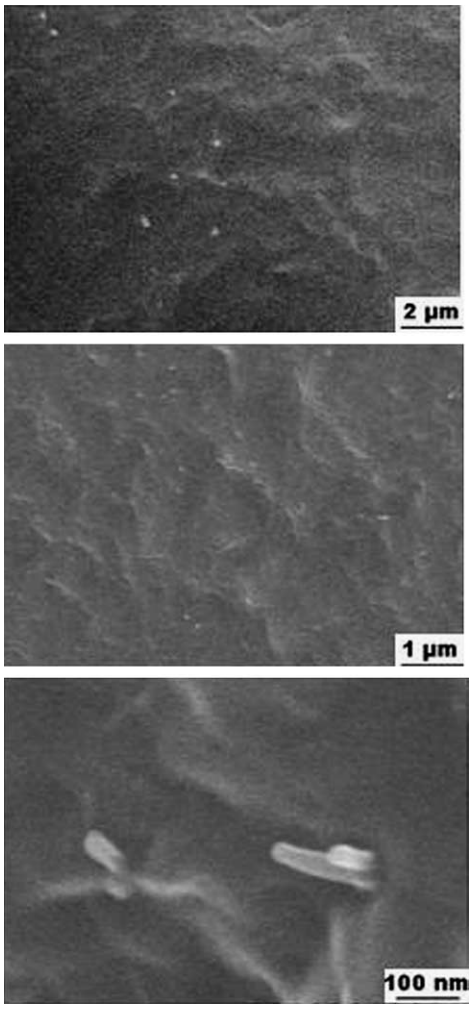

Fig. 4. SEM photographs of PA6/MWNT (top, 20000X) and PA6/MWNT-COOH (middle, 10000X; bottom, 100000X).

shows the scattered intensity as a function of the scattering vector, q, where $q = 4\pi/\lambda \sin(\theta/2)$, λ being the wavelength and θ the scattering angle. The three curves represent the neat PA6 and the two composites discussed above. Simple observation of these data reveals:

1. There is no morphological difference between PA6/MWNT and PA6/MWNTCOOH.
2. There is no evidence of rod-like morphology. That is, there is no region where the data follow a power-law with exponent -1, which would characterize scattering from a linear object.
3. For the region $q > 0.03$ Å^{-1}, the data are dominated by scattering from the matrix. The peak near 0.07 Å^{-1} presumably represents scattering from lamellar polymer crystallites. This crystalline morphology does not appear to be appreciably altered by the presence of the CNTs.

Further insight into the morphology of the CNTs is gained by subtraction of the matrix scattering (Fig. 7). These background-subtracted data are rather featureless showing a

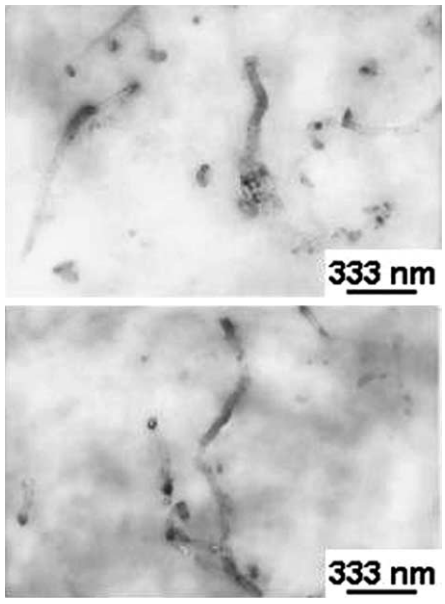

Fig. 5. TEM imagines of PA6/MWNT (top, 30000X) and PA6/MWNT-COOH (bottom, 30000X).

crossover from a slope of -1.6 at low q to -4 at large q. The slope of -4 is the signature of a smooth interface as would be expected at the CNTs surface. The crossover q value ($q = 0.008$ Å^{-1}), which corresponds to a length scale of $q^{-1} = 125$ Å (12.5 nm), a reasonable size for the radius of the CNTs (Fig. 5). The limiting slope of -1.6 at low q shows that the scattering entities are not linear objects, which would give a slope of -1 (dotted line in Fig. 7).

The absolute intensity reveals the state of dispersion. To illustrate this fact, the data are compared to that expected

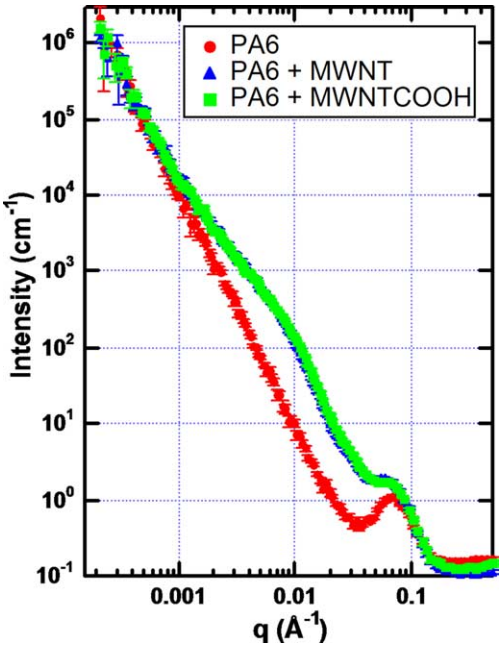

Fig. 6. X-ray scattering profile for PA6/CNTs composites compared to scattering from the neat PA6.

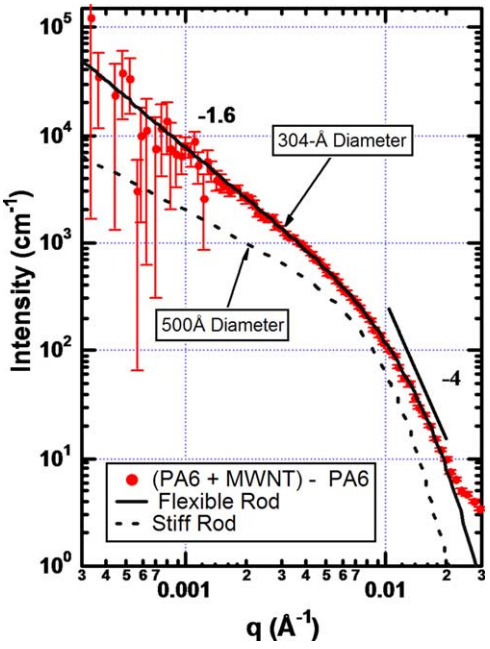

Fig. 7. Matrix-background subtracted USAXS from PA6/MWNT compared to stiff and flexible rod models.

from a dilute suspension of stiff rods (dotted line in Fig. 7). For the stiff-rod model a diameter of 500 Å (50 nm) was assumed. The rod length was taken to be infinite, or at least beyond the resolution of the instrument. The densities of MWNT and PA6 were assumed to be 1.0 and 1.14 g/cm^3 respectively. If a higher density is assumed for the MWNT, the predicted curve decreases in intensity.

The stiff-rod model in Fig. 7 is based on a simplified model of a rigid rod (Appendix A). The simplified-rod form factor matches the exact form factor of a rod except for $q > 1/R$, where R is the rod radius. The exact form factor shows oscillations in this q regime, which are seldom seen in real data due to polydispersity in the rod diameters. These oscillations are suppressed in the simplified model. Otherwise, the simplified model matches the exact calculation.

For the dotted line in Fig. 7, $R = 250$ Å (25 nm), and the length is essentially infinite ($L = 10^6$ Å). Although the calculation does not match the data, it is within a factor of 2 in the crossover region where the data is very sensitive to the rod diameter. That is, the observed intensity is only marginally larger than that expected for an isolated rod, indicating good dispersion.

The discrepancy between the data and the calculation for isolated stiff rods could be due to several factors. A distribution of rod diameters could be included to match the data in the crossover region. If the rods were aggregated side-by-side, the scattering entity would essentially be a rod of larger diameter. Attempts to match the data with larger diameter rods, however, lead to poorer matches to the data. Such models also will never match the observed slope (P_2 in the model in the appendix) of 1.6 at small q. The deviation of P_2 from 1 is probably due to the flexibility in the rods.

The simplest concept that explains the data is that the rods are flexible. If the rods followed a self-avoiding walk, for example, $P_2 = 5/3$, close to the observed value. To model the flexible chain, we developed a wormlike-rod model based on fractal ordering of short rod-like segments with persistence length L_p. That is, the fundamental 'mononmer' or worm segment is a short rod of length $L = L_p$ and radius R. These rod-like segments are then fractally correlated on larger scales with mass fractal dimension, D. Eqs. (A1) and (A2) in Appendix A are then used to capture the form factor of the rod segments with $L = L_p$.

Fractal correlations of the stiff segments are introduced using the structure factor, $S(q)$, proposed by Teixeira [31]:

$$S(q, D, \xi, L_p) = 1 + \frac{D \exp(\Gamma(D-1))\sin(D-1)\tan^{-1}(q\xi)}{(qL_p)^D[1 + (q\xi)^{-2}]^{(D-1)/2}}$$

where ξ is the correlation range (essentially infinite in our case since it is beyond the resolution of the instrument). The over-all wormlike rod scattering function, I_{WLR}, is then:

$$I_{WLR} = S(q, D, \xi, L_p)[I_1(q, R, L_p) + I_2(q, R, L_p)]$$

where I_1 and I_2 are defined in the appendix. This function, which is plotted as the solid line in Fig. 7, matches the data very well in the region $q < 0.02$ Å^{-1} with $R = 152$ Å (15.2 nm), $L_p = 800$ Å, $D = 1.57$, $\xi = \infty$. Again we had to assume a carbon density of 1.0 g/cm^3 to fit the data. Since the R is about that observed in Fig. 5, the match of the wormlike model to the data indicates complete dispersion of the CNTS in the matrix.

It should be realized that other dispersed-filler models can fit the data, so the correspondence observed here does not prove rod flexibility. If the rods were clustered into aggregates or nets with fractal correlations, for example, the scattering could be modeled by exactly the same function as used here. The effect on mechanical properties would also be similar (see below).

These results indicate that the marginal enhancement of mechanical properties observed for PA6/CNTs is not due to poor dispersion. Rather, the CNTs modified or not, are quite flexible in a fashion like Fig. 5. In this case, the mechanical enhancement is dependent on the flexural or bending modulus of the rod, not the tensile modulus. Given the flexibility of the rods, the flexural modulus might be rather low, leading to marginal enhancement of the composite mechanical properties.

4. Conclusions

PA6/CNTs composites are prepared using the typical PA6 hydrolytic polymerization conditions. CNTs are ultrasonically pre-dispersed in the polymerizable master solution to achieve the homogeneous dispersion of CNTs in PA6 matrix. Adding 0.5 wt% CNTs has little effect on the molecular weight of PA6. The tensile strength and storage

modulus of PA6/CNTs composites are improved slightly, and CNTs do influence the crystallization and glass transition behavior. SEM, TEM and USAXS demonstrate MWNT and MWNTCOOH are well dispersed in PA6 matrix. Further fitting of USAXS data indicates CNTs exhibit flexible-rod morphology. This flexible morphology reduces the mechanical property enhancement since the bending rather than the tensile modulus controls the composite properties.

Acknowledgements

The authors gratefully acknowledge the financial support of the Major Basic Research Projects of China (Grant 2003CB615600). We thank Pete Jemian for guidance in using the USAXS instrument at UNICAT and for development of the analysis software. The UNICAT facility is supported by the US DOE under Award No. DEFG02-91ER45439 (University of Illinois at Urbana-Champaign), the Oak Ridge National Laboratory (US DOE Contract DE-AC05-00OR22725), the National Institute of Standards and Technology (US Department of Commerce) and UOP LLC.

Appendix A: An approximate form factor for a stiff rod

The mathematical form of the simplified stiff-rod model is that of a 2-level unified scattering function [32,33].

$$I(q,R,L) = I_1(q,R,L) + I_2(q,R,L) \tag{A1}$$

Level-1 scattering, $I_1(q)$, is from the short-scale structure and is dependent primarily on the radius, R, of the rod. The level-2 intensity, $I_2(q)$, is from the large-scale linear structure and is dependent on R and the length, L, of the rod. The intensity, I_X, from level X is:

$$I_X(q,R,L) = G_X \exp\left(\frac{-(qR_{gx})^2}{3}\right) + \left(\frac{B_X}{q^{P_X}}\right)\left(\left[\operatorname{erf}\left(\frac{qR_{gx}}{\sqrt{6}}\right)\right]^{3P_X} \exp\left(\frac{(R_{cox}q)^2}{3}\right)\right) \tag{A2}$$

The exponential term will be recognized as the Guinier term and the second power-law term is Porod scattering. The factor containing the error function, erf, assures a smooth crossover between the Guinier and Porod regimes. For the stiff-rod model:

$$G_2 = \varphi(1-\varphi)(\Delta\rho)^2\pi R^2 L$$

$$R_{g2} = \left(\frac{R^2}{2} + \frac{L^2}{12}\right)^{1/2}$$

$$B_2 = \frac{\pi G_2}{L}$$

$$P_2 = 1$$

$$G_1 = \frac{2G_2R}{3L}$$

$$R_{g1} = R_{co2} = \frac{\sqrt{3}}{2}R$$

$$B_1 = 4G_2(L+R)/R^3L^2$$

$$P_1 = 4$$

$$R_{co1} = 0$$

Here ϕ is the volume fraction and $\Delta\rho$ is the X-ray contrast (difference in the X-ray scattering length densities of the filler and the matrix). Level 1 will be recognized as Porod scattering from a smooth surface in that $P_1 = 4$. The Porod constant B_1 is proportional to the interfacial area per unit volume, $2\phi(R^{-1}+L^{-1})$. In the second power-law region the slope is $P_2 = -1$ as expected for a rod and the prefactor, B_2, scales as the cross sectional area (R^2). R_{g2} is the radius-of-gyration of the rod. R_{g1} is chosen to match the exact rod model in the crossover region near $q = 1/R$.

References

[1] Iijima S. Nature 1991;354:56–8.
[2] Popov VN. Mater Sci Eng R 2004;43(3):61–102.
[3] Demczyk BG, Wang YM, Cumings J, Hetman M, Han W, Zettl A, et al. Mater Sci Eng A 2002;334:173–8.
[4] Andrews R, Weisenberger MC. Curr Opin Solid State Mater Sci 2004; 8(1):31–7.
[5] Breuer O, Sundararaj U. Polym Compos 2004;25(6):630–45.
[6] Shaffer MSP, Windle AH. Adv Mater 1999;11(11):937–41.
[7] Bin Y, Kitanaka M, Zhu D, Matsuo M. Macromolecules 2003;36(16): 6213–9.
[8] Ruan SL, Gao P, Yang XG, Yu TX. Polymer 2003;44(19):5643–54.
[9] Paiva MC, Zhou B, Fernando KAS, Lin Y, Kennedy JM, Sun Y-P. Carbon 2004;42(14):2849–54.
[10] Sennett M, Welsh E, Wright JB, Li WZ, Wen JG, Ren ZF. Appl Phys A 2003;76(1):111–3.
[11] Zou Y, Feng Y, Wang L, Liu X. Carbon 2004;42(2):271–7.
[12] PÖtschke P, Bhattacharyya AR, Janke A. Eur Polym J 2004;40(1): 137–48.
[13] Bhattacharyya AR, Sreekumar TV, Liu T, Kumar S, Ericson LM, Hauge RH, et al. Polymer 2003;44(8):2373–7.
[14] Meincke O, Kaempfer D, Weickmann H, Friedrich C, Vathauer M, Warth H. Polymer 2004;45(3):739–48.
[15] Sandler JKW, Pegel S, Cadek M, Gojny F, van Es M, Lohmar J, et al. Polymer 2004;45(6):2001–15.
[16] Liu TX, Phang IY, Shen L, Chow SY, Zhang W-D. Macromolecules 2004;37(19):7214–22.
[17] Kumar S, Dang TD, Arnold FE, Bhattacharyya AR, Min BG, Zhang X, et al. Macromolecules 2002;35(24):9039–43.

[18] Velasco-Santos C, Martĺnez-Hernández AL, Fisher FT, Ruoff R, Castaño VM. Chem Mater 2003;15(23):4470–5.
[19] Tong X, Liu C, Cheng H-M, Zhao H, Yang F, Zhang X. J Appl Polym Sci 2004;92(6):3697–700.
[20] Nogales A, Broza G, Roslaniec Z, Schulte K, Šics I, Hsiao BS, et al. Macromolecules 2004;37(20):7669–72.
[21] Park SJ, Cho MS, Lim ST, Choi HJ, Jhon MS. Macromol Rapid Commun 2003;24(18):1070–3.
[22] Jia Z, Xu C, Liang J, Wei B, Wu D, Wang Z, et al. J Tsinghua Univ 2000;40(4):14–16.
[23] Xia H, Wang Q, Qiu G. Chem Mater 2003;15(20):3879–86.
[24] Mehta RH. In: Brandrup J, Immergut EH, Grulke EA, editors. Polymer handbook, 4th ed, vol. 5. New York: Wiley; 1999. p. 128–30.
[25] Liu J, Rinzler AG, Dai H, Hafner JH, Kelley Bradley R, Boul PJ, et al. Science 1998;280:1253–6.
[26] Zhao C, Ji L, Liu H, Hu G, Zhang S, Yang M, et al. J Solid State Chem 2004;177(12):4394–8.
[27] Schaefgen JR, Flory PJ. J Am Chem Soc 1948;70(8):2709–18.
[28] Sun Y, Wilson SR, Schuster DI. J Am Chem Soc 2001;123(22):5348–9.
[29] Ausman KD, Piner R, Lourie O, Ruoff RS, Korobov M. J Phys Chem B 2000;104(38):8911–5.
[30] Jia Z, Xu C, Liang J, Wei B, Wu D, Zhu C. Xinxing Tan Cailiao 1999; 14:32–6.
[31] Teixeira J. J Appl Cryst 1988;21(6):781–5.
[32] Beaucage G, Schaefer DW. J Non-Cryst Solids 1994;172:797–805.
[33] Beaucage G. J Appl Cryst 1995;28(6):717–28.